Astron. Astrophys. 329, 1059–1074 (1998)

ASTRONOMY AND ASTROPHYSICS

Circumstellar molecular radio line intensity ratios

H. Olofsson[1], **M. Lindqvist**[2], **L–Å. Nyman**[2,3], **and A. Winnberg**[2]

[1] Stockholm Observatory, S-133 36 Saltsjöbaden, Sweden
[2] Onsala Space Observatory, S-439 92 Onsala, Sweden
[3] ESO/La Silla, Casilla 19001, Santiago 19, Chile

Received 13 June 1997 / Accepted 3 September 1997

Abstract. We have observed a sample of 61 AGB–stars (39 M–stars and 22 C–stars) in circumstellar CO, CS, HCN, SiO, SiS, and SO radio line emission. The main results presented are based on the use of line intensity ratios, a well defined observational quantity that can be used to infer important conclusions as well as to provide constraints on models. Taken together the data are fully consistent with the facts that for this sample the circumstellar envelopes have the same basic chemistry (i.e., C/O$<$1 or $>$1) as the central stars, and that the mass loss rates have not changed drastically over periods between 10^2–10^3 years. The HCN($J = 1 \rightarrow 0$)/SiO($J = 2 \rightarrow 1$) intensity ratio discriminates unambiguously between "normal" circumstellar envelopes with C/O$<$1 (O–CSEs) and $>$1 (C–CSEs), while the CS($J = 2 \rightarrow 1$), HCN($J = 1 \rightarrow 0$), SiO($J = 2 \rightarrow 1$), and SiS($J = 5 \rightarrow 4$) intensity ratios with respect to CO($J = 1 \rightarrow 0$) are not perfect for this purpose, and neither is the SiS($J = 5 \rightarrow 4$)/SiO($J = 2 \rightarrow 1$) intensity ratio. The data further shows that SO and the C-bearing molecule HCN are ubiquitously present in O–CSEs, and that their line intensities in O–CSEs are qualitatively consistent with the fact that the molecules are formed in a photo–induced circumstellar chemistry in a quantity that depends on the mass loss rate. Hence, both species can in principle be used to estimate the mass loss rate, and the tight relation between the SO($J_K = 3_2 \rightarrow 2_1$) and CO($J = 1 \rightarrow 0$) intensities in O–CSEs shows that SO line emission may even be a good mass loss rate estimator. On the contrary, the SiO($J = 2 \rightarrow 1$) luminosity appears to be essentially independent of the mass loss rate in O–CSEs, possibly due to a larger influence from molecular adhesion onto grains. These results explain why the HCN($J = 1 \rightarrow 0$)/SiO($J = 2 \rightarrow 1$) intensity ratio increases with the mass loss rate in O–CSEs, and there is no need to invoke e.g. a spread in C/O–ratios for the M–stars to explain the large range of this ratio.

Maser emission is very likely present in the HCN($J = 1 \rightarrow 0$) line in C–CSEs, and it seems to be sensitively dependent on the mass loss rate, i.e., it appears only for $\dot{M} \lesssim 5 \times 10^{-7}\,\mathrm{M}_\odot\,\mathrm{yr}^{-1}$. Based on time monitoring of this emission towards the C–stars W Ori and X TrA, we suggest that the strongest maser features are due to radial amplification in the $F = 2 \rightarrow 1$ transition. The predominance of redshifted maser emission could be caused by an additional amplification in the $F = 1 \rightarrow 1$ transition. We find no evidence for a similar maser in O–CSEs.

Key words: masers – stars: carbon – circumstellar matter – stars: mass–loss – stars: AGB, post–AGB – radio lines: stars

1. Introduction

An impressive number of different molecular species (≈60) and their isotopic variants have been found in the circumstellar envelopes (CSEs) that are formed around asymptotic giant branch (AGB) stars through their intense mass loss (Olofsson 1997a). Some of these molecules are of photospheric origin, but the majority are produced through various chemical processes in the envelope itself. This chemistry depends primarily on the chemical composition of the gas (i.e., C/O$<$1 or $>$1), but the physical conditions also change as the central star evolves along the AGB and beyond. The relative simplicity of the envelopes, i.e., their geometry and kinematics, and the large variety in their physical and chemical characteristics, make them excellent laboratories for studying molecular formation processes in an astrophysical context. However, the circumstellar molecules are also important probes in the study of late stellar evolution (Olofsson 1997a,c).

The photospheric species are produced in an equilibrium chemistry in the atmosphere of the central star (see e.g., Tsuji 1964, 1973; Lafont et al. 1982; Glassgold & Huggins 1983; Cherchneff & Barker 1992). The main problem is that the molecular abundances normally vary with the height in the atmosphere, and it is not clear which abundances to adopt for the escaping gas. Furthermore, there may be significant departures from equilibrium due to e.g. shocks propagating through the atmosphere and dust formation. These parent molecules are eventually photodissociated, which results in the direct formation of the photodissociation products, as well as the indirect formation of other species by providing the ingredients of a circumstellar chemistry. The latter has been studied theoretically in a number of papers, both for the chemical compositions of O– (see e.g.,

Send offprint requests to: H. Olofsson (hans@astro.su.se)

Scalo & Slavsky 1980; Huggins & Glassgold 1982; Nejad & Millar 1988; Nercessian et al. 1989; Millar & Olofsson 1993; Charnley et al. 1995; Willacy & Millar 1997) and C–CSEs (see e.g., Lafont et al. 1982; Nejad & Millar 1987; Glassgold et al. 1992; Cherchneff & Glassgold 1993; Millar & Herbst 1994).

Circumstellar molecules have also been extensively observed, both in the form of surveys in a single molecular species and in the form of searches for various molecular species in a limited number of carefully selected sources (Olofsson 1997b). We will here concentrate on studies aimed at estimating molecular abundances. Olofsson et al. (1993b) performed a survey of HCN, CN, and CS in a sample of bright carbon stars (57 objects, 39 detections of HCN). They found that the circumstellar HCN abundance have a reasonable dependence on the corresponding photospheric abundance, and that the circumstellar CN is a photodissociation product, but they also concluded that there is likely to be considerable systematic errors in their abundance estimates caused by imperfections of the model for the circumstellar emission. The latter was further emphasized by Izumiura et al. (1995) who pointed out that the brightnesses of the HCN($J = 1 \rightarrow 0$) line in C–CSEs are not consistent with the expected sizes of the emitting regions. Bujarrabal et al. (1994a) estimated a number of molecular abundances (e.g., HCN, CS, SiO, and SiS) in a sample of 16 C–CSEs, and Bachiller et al. (1997) estimated the CN abundances in 26 C–CSEs. Nyman et al. (1993) compared more than 10 circumstellar molecular abundances for the high mass loss C–stars IRC+10216 and IRAS15194–5115. HCN has also been extensively observed in O–CSEs (≈20 detections; Lindqvist et al. 1988, 1992; Nercessian et al. 1989; Bujarrabal et al. 1994a), and to a lesser extent has CN (2 AGB–stars and 3 supergiants; Olofsson et al. 1991; Bachiller et al. 1997). Recently, Charnley & Latter (1997) searched a number of O–CSEs for C_2H and CH_3OH without success. Species considerably more characteristic for, and probably unique to, O–CSEs are SO and SO_2, and they have also been detected in ≈20 sources each (see e.g., Sahai & Wannier 1992; Omont et al. 1993). Bieging & Latter (1994) extended this type of work to CSEs around S–stars, where they concentrated on HCN and SiO. However, the conclusion to be drawn from these studies is that absolute abundances are fairly uncertain, by at least an order of magnitude, and can at best be used for studying trends, or differences in the chemistry between O– and C–CSEs. More sophisticated models are required in order to make significant progress here, but some of the crucial observational data are still largely missing, e.g., direct measurements of the brightness distributions.

Bujarrabal et al. (1994a,b) showed that even simple molecular line intensity ratios, if properly chosen, may be used to infer important conclusions. For instance, it is possible to distinguish between "normal" O– and C–CSEs (Bujarrabal et al. 1994b; by a "normal" CSE we here mean one that has been produced by a relatively constant mass loss of constant chemical composition over a relatively long time scale, $\lesssim 10^3$ years), and Olofsson et al. (1993b) and Bujarrabal & Cernicharo (1994) used them to identify anomalous CSEs. The use of line intensity ratios has the advantage of requiring no assumptions about a circumstellar model, but it also limits the type of conclusions that can be drawn. In this paper we proceed along this line, thereby considerably strengthening some of the conclusions drawn by Bujarrabal et al. (1994a,b), as well as obtaining a number of new results that will serve as constraints on chemical and circumstellar models.

Table 1. Overview of the observations

	Freq.	O–CSEs		C–CSEs	
	[GHz]	detected	negative	detected	negative
CO($J = 1 \rightarrow 0$)	115.3	37	- [a]	22	-
HCN($J = 1 \rightarrow 0$)	88.6	19	20	22	-
SiO($J = 2 \rightarrow 1$)	86.8	29	-	12	10
SO($J_K = 2_2 \rightarrow 1_1$)	86.1	-	4	-	-
SO($J_K = 3_2 \rightarrow 2_1$)	99.3	16	5	-	-
SiS($J = 5 \rightarrow 4$)	90.8	3	3	7	6
CS($J = 2 \rightarrow 1$)	98.0	2	5	15	7

[a] Two M–stars were not detected in CO because of problems with interfering interstellar CO emission

2. Sample

We report results on circumstellar CO, CS, HCN, SiO, SiS, and SO radio line observations of 61 AGB–stars, 39 M–stars (≈70% Miras and ≈30% Semiregulars) and 22 C–stars (≈40% Miras and ≈60% Semiregulars).

The M–stars were chosen among stars spectroscopically classified as M–stars (Kholopov et al. 1985), and/or have emission in at least one of the masing lines of OH, H_2O, or SiO (Engels & Heske 1989; Benson et al. 1990), and/or have an LRS-class 2n (Olnon & Raymond 1986). This makes it very likely that the associated CSEs also have elemental compositions where C/O$<$1. The majority of the C–stars are well known carbon stars, e.g, a fair fraction (≈55%) of them belong to the sample studied by Lambert et al. (1986), and except for S Cep and RV Cyg they have an LRS–class 4n. The associated CSEs very likely have elemental compositions where C/O$>$1. From now on we will refer to CSEs around M– and C–stars as O– and C–CSEs, respectively, assuming that the C/O-ratio of the central star and the CSE agree with each other. As will be shown, there is nothing in our data that contradicts this assumption. The variability type was taken from Kholopov et al. (1985). We have used the best coordinates available at the time of the observation (see e.g., Loup et al. 1993). Only in a few cases have we retreated to the IRAS coordinates.

The distances, D, for the M–stars are obtained by integrating visual, near-infrared, and IRAS data assuming a luminosity of 5000 $L_\odot$ for the Semiregulars (Kerschbaum & Hron 1996), using the period–luminosity relation obtained by Whitelock et al. (1994) for the Miras, and assuming a luminosity of 10^4 $L_\odot$ for those stars where the variability class is not known. For the optically bright C–stars we adopt the method used in Olofsson et al. (1993a), i.e., we assume an absolute K–magnitude of -8.1, while for the more extreme C–stars (V384 Per, 07454–

7112, CW Leo, RW LMi, 15082–4808, 15194–5115) we adopt values from the literature (e.g., Sopka et al. 1989; Loup et al. 1993).

3. Observations

An overview of the observations are given in Table 1 and the observational results are given in Table 2. All data have been obtained with the Onsala 20m telescope (OSO), Sweden, and the Swedish-ESO Submillimetre Telescope (SEST) on La Silla, Chile, by us (this paper; Lindqvist et al. 1988, 1992) or by others (Nyman et al. 1992; Olofsson et al. 1993a,b; Kerschbaum et al. 1996; Larsen et al. 1997; Nyman & Olofsson 1997) during the period 1987–1997. For each star the same telescope has been used for all observed transitions. This data base is larger than the one used in a similar study by Bujarrabal et al. (1994a): 30 AGB–stars, 14 M–stars (e.g., 9 detections of HCN, 7 detections of SO), 16 C–stars (e.g., 10 detections of SiO).

The line intensities, integrated over velocity, are given in the main beam brightness scale, i.e., the antenna temperature has been corrected for the atmospheric attenuation (using the chopper wheel method) and divided by the main beam efficiency. The latter is ≈0.6–0.5 (≈0.4–0.3 for data obtained before March 1993) in the frequency range 86–115 GHz for OSO, and ≈0.75 in the same frequency range for SEST. The upper limits are calculated using the peak–to–peak value, $T_{\rm pp}$, of a spectrum with a velocity resolution reduced to twice the expansion velocity of the CSE, i.e., $I_{\rm upper} = 2T_{\rm pp}v_{\rm e}$. This should provide a conservative upper limit. The gas expansion velocities, $v_{\rm e}$, are obtained as half the full width at zero power of the CO($J = 1 \rightarrow 0$) line profiles. The telescope used is indicated by O for OSO and S for SEST. The beam widths lie in the ranges 33″–42″ for OSO and 45″–60″ for SEST, respectively.

New detections not yet reported in the literature are CS: V384 Per, S Cep (from Larsen et al. 1997) and 07454–7112, 15082–4808 (from Nyman & Olofsson 1997); HCN: R Leo, CIT4, IRC+50137; SiO: R For, V384 Per, R Lep, R Vol, RV Aqr, and 07454–7112, 15082–4808 (from Nyman & Olofsson 1997); SO: R Dor, GX Mon, W Hya, RS CrA, R Aql, CIT4, IRC+70066; SiS: WX Psc, and V384 Per, V Cyg (from Larsen et al. 1997), and 07454–7112, 15082–4808 (from Nyman & Olofsson 1997). Spectra of the new detections are presented in Fig. 1 [except those that will be published in Larsen et al. (1997) and Nyman & Olofsson (1997)].

4. Molecular line intensity ratios

The line intensity ratios to be discussed are HCN ($J = 1 \rightarrow 0$) / CO ($J = 1 \rightarrow 0$), SiO ($J = 2 \rightarrow 1$) / CO($J = 1 \rightarrow 0$), HCN ($J = 1 \rightarrow 0$) / SiO ($J = 2 \rightarrow 1$), and SO ($J_K = 3_2 \rightarrow 2_1$) / CO($J = 1 \rightarrow 0$). Line intensity ratios involving CS and SiS are not discussed at any lengths due to the small number of detections of these species in O–CSEs. The results of the line intensity ratios are summarized in Table 3. We find no evidence that the molecular line intensity ratios are dependent on the beam size (e.g., due to partial resolution of the brightness distributions), and therefore OSO and SEST data are not separated in the analysis. This also means that the results should apply to any telescope as long as the effect of beam filling can be ignored.

We have not estimated the formal error of each individual line intensity ratio for the following reason. We found the intensity of the calibration sources to be repeatable at the ±10% level at both OSO and SEST. If we include pointing uncertainties the intensity scale is estimated to have an uncertainty of ±15%. The absolute calibration of the intensity scale is not of interest here since we are only using line intensity ratios obtained using data from the same telescope. Some of the lines are quite weak (in practice those for which $I < 1\,{\rm K\,km\,s^{-1}}$), and for those we estimate that the line intensity ratio (which always involve one line that is reasonably strong) is uncertain by at most ±50%. Thus, we expect the uncertainties to lie in the range ±20% to ±50%. This will have no effect on the conclusions drawn in this paper.

We will first introduce a simple mass loss rate measure, adequate for discussing the dependences of various molecular line intensity ratios on the mass loss rate of the central object.

4.1. A mass loss rate measure

Amongst other things, we are interested in looking at the dependences of the line intensity ratios on the mass loss rate. To obtain the absolute mass loss rate of a star from e.g. its CO line emission requires relatively detailed modelling (see e.g., Sahai 1990; Kastner 1992; Kwan & Webster 1993; Groenewegen 1994; Justtanont et al. 1994). However, we are only interested in trends and not in the absolute mass loss rates of the individual stars. We have therefore decided to compare our results with the simple mass loss rate measure $I_{\rm CO}v_{\rm e}D^2$ [it is reasonable to assume that this expression contains all the observational quantities, as well as the main functional dependence of the mass loss rate on them, that are required to estimate the mass loss rate, see e.g., Kastner 1992)], where $I_{\rm CO}$ is the velocity–integrated intensity of the CO($J = 1 \rightarrow 0$) line in $\rm K\,km\,s^{-1}$, $v_{\rm e}$ is given in $\rm km\,s^{-1}$, and D is given in kpc (we will in the following not repeat the somewhat awkward unit of the mass loss rate measure, $\rm K\,km^2\,s^{-2}\,kpc^2$). In doing this we have scaled the SEST CO intensities to the Onsala scale by simply assuming that the intensity increases in proportion to the telescope area. In Fig. 2 we compare $I_{\rm CO}v_{\rm e}D^2$ with mass loss rate estimates obtained from model work (Sopka et al. 1989; Kahane & Jura 1994; Justtanont et al. 1994), and, for the low–$\dot{M}$ C–CSEs, from Loup et al. (1993). There is clearly a good correlation although the relation is weaker than a linear one, so that a change in the mass loss rate measure by three orders of magnitude corresponds to a change in the mass loss rate by about two orders of magnitude. There is no significant difference between O– and C–CSEs in this respect. A fit to the data (irrespective of the chemistry) results in

$$\dot{M} = 2.0 \times 10^{-7}\,(I_{\rm CO}v_{\rm e}D^2)^{0.59}\ {\rm M_\odot\,yr^{-1}}, \qquad (1)$$

with a correlation coefficient of 0.92.

In Fig. 3 we plot our stars in a two–colour diagram based on the IRAS–fluxes. The area of the symbols are proportional

Table 2. Observational results

Source	IRAS	Var.	D [pc]	Tel.[a]	v_e [km s^{-1}]	I_{mb} [K km s^{-1}]						
						CO(1-0)[b]	CS(2-1)	HCN(1-0)	SiO(2-1)	SiS(5-4)	SO(3_2-2_1)	SO(2_2-1_1)
M–stars:												
IRC+40004	00042 + 4248	M	410	O	19.3	24.8		<0.6	1.1			
T Cas	00205 + 5530	M	360	O	10.6	2.0		<0.9				
WX Psc	01037 + 1219	M	600	O	19.3	52.0	<0.8	3.7	9.7	1.4	5.8	<0.4
BD+44398	01556 + 4511		250	O	9.4	3.9		<1.1				
CIT4	02316 + 6455		290	O	19:	15:		0.7:	1.7		1.4:	
R Hor	02522 − 5005	M	280	S	5.5	2.5		<0.4				
IK Tau	03507 + 1115	M	250	O	18.5	58.2	0.5	3.5	15.8	0.3	3.6	<0.4
R Dor	04361 − 6210	SRb	70	S	6.2	5.0		0.6	13.5		0.5	
TX Cam	04566 + 5606	M	380	O	21.5	21:	1.0	4.8	13.0	0.6	2.1	<0.6
IRC+50137	05073 + 5248	M	410	O	18.0	19.7		0.9	1.9		1.2	
IRC+60154	05151 + 6312		330	O	18.8	5.3		<0.6	0.8			
U Aur	05388 + 3200	M	610	O		IS		<0.3	0.9			
IRC+70066	05411 + 6957		470	O	18.5	20.0		1.3	3.3	<0.3	0.9	
V Cam	05559 + 7430	M	650	O	15.1	3.7		<0.6	1.0			
IRC+60169	06300 + 6058		490	O	14.4	16.4	<0.6	1.2	4.3		1.2	
GX Mon	06500 + 0829	M	540	O	18.7	48.6	<1.0	2.3	9.2		2.9	
RS Cnc	09076 + 3110	SRc:	100	O	7.0	7.3		<0.7				
IRC–20197	09429 − 2148	M:	340	S	11.5	1.4		<0.3				
R Leo	09448 + 1139	M	130	O	7.5	2.4		0.4	4.5		<0.4	
R Crt	10580 − 1803	SRb	180	S	10.3	5.0		0.5	5.7			
RT Vir	13001 + 0527	SRb	190	O	9.2	5.1		0.3	4.0		<0.4	
SW Vir	13114 − 0232	SRb	140	O	8.1	10.2		<0.8	3.5		<0.5	
R Hya	13269 − 2301	M	150	S	4.0	0.6		<0.4	4.2			
W Hya	13462 − 2807	SRa	90	S	7.3	0.8		0.4	7.7		0.2:	
RX Boo	14219 + 2555	SRb	150	O	9.8	13.7		0.5	9.3		1.0	
S CrB	15193 + 3132	M	380	O	7.9	2.6		<0.6				
X Her	16011 + 4722	SRb	160	O	6.2	3.9		<0.4	2.6		<0.5	
g Her	16269 + 4159	SRb	110	O	9:	1.7:		<1.1				
MW Her	17334 + 1537	M	670	O	14.4	5.9		<0.7				
IRC+10365	18349 + 1023	M	750	O	16.2	21.4	<0.6	2.0	6.0	<0.3	2.2	<1.3
IRC–30398	18560 − 2954	M:	390	S	19.6	10.4		0.4	1.2		<0.2	
RS CrA	18595 − 3947	M:	210	S	18.7	14.9		1.7	5.2		1.3	
R Aql	19039 + 0809	M	230	O		IS		<0.6	5.0		1.1	
RR Aql	19550 − 0201	M	430	O	7.2	4.2		<0.5	0.9			
IRC–10529	20077 − 0625	M:	270	O	16.0	28.0		1.0	2.9		3.7	
T Cep	21088 + 6817	M	220	O	6.9	1.7		<1.1	0.6			
EP Aqr	21439 − 0226	SRb	140	S	9.8	5.1		<1.0				
TW Peg	22017 + 2806	SRb	220	O	9.8	2.3		<1.0				
R Cas	23558 + 5106	M	220	O	14.3	14.4	<0.4	1.3	8.6	<0.4	1.7	
C–stars:												
R For	02270 − 2619	M	670	S	16.3	4.8	0.6	2.0	0.4			
V384 Per	03229 + 4721	M	650	O	14.2	25.5	6.9	8.0	1.2	0.4		
U Cam	03374 + 6229	SRb	500	O	24.7	5.8	1.6	3.9	<0.4	<0.3		
ST Cam	04459 + 6804	SRb	510	O	8.6	2.0	<0.5	2.3	<0.5			
R Lep	04573 − 1452	M	430	S	17.0	6.2	<0.3	2.3	0.5			
W Ori	05028 + 0106	SRb	360	O	11.1	2.7	<0.8	4.6	<0.7			
Y Tau	05426 + 2040	SRb	500	O	15.2	7.0	<0.4	3.5	<1.5			
UU Aur	06331 + 3829	SRb	300	O	10.9	7.9	<0.5	5.5	<0.5			
R Vol	07065 − 7256	M	820	S	18.5	4.9	1.3	1.9	0.8:	<0.3		
07454–7112	07454 − 7112		750	S	13.6	24.1	2.3	4.1	0.6	0.8		
CW Leo	09452 + 1330	M	150	O	14.2	310.7	130.0	227.0	29.9	40.6		
RW LMi	10131 + 3049	SRa	390	O	15.8	75.8	19.2	28.4	3.8	1.3		
Y CVn	12427 + 4542	SRb	290	O	8.4	4.5	0.7	9.7	<0.4	<0.3		
RY Dra	12544 + 6615	SRb:	470	O	7.3	2.4	0.9	3.4	<0.4	<0.2		
15082–4808	15082 − 4808		670	S	20.4	38.3	8.6	10.7	2.1	1.1		
X TrA	15094 − 6953	Lb	320	S	7.8	2.5	<0.4	3.1	<0.3			
15194–5115	15194 − 5115		470	S	22.2	49.0	12.1	17.2	5.4	2.4		
V Aql	19017 − 0545	SRb	390	O	7.6	3.2	0.2	1.3	<0.4			
V Cyg	20396 + 4757	M	580	O	13.1	34.0	6.3	9.0	1.2	0.3:		
RV Aqr	21032 − 0024	M	820	S	14.9	8.0	1.3	2.3	0.7	<0.4		
S Cep	21358 + 7823	M	440	O	22.0	16.3	7.5	11.8	1.7	<0.2		
RV Cyg	21412 + 3747	SRb	490	O	13.3	4.8	<0.5	2.0	<0.6			

[a] O = OSO 20m telescope, S = 15m SEST

[b] IS = confusion due to interstellar CO emission

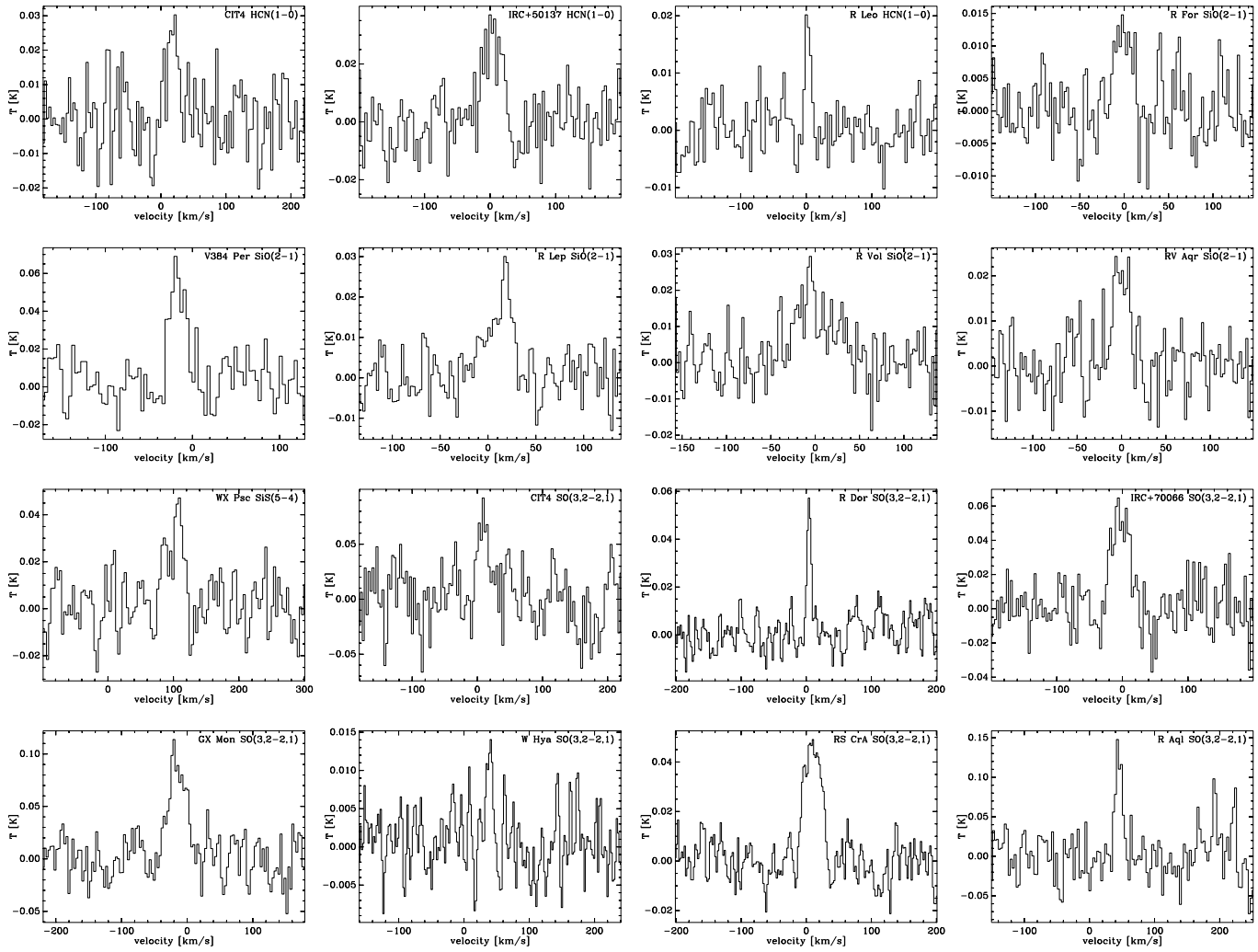

Fig. 1. Spectra of the new detections. The intensity scale is given in main beam brightness temperature. The velocity scale of the WX Psc SiS($J = 5 \rightarrow 4$) spectrum is shifted by 94.1 km s^{-1}

Table 3. Line intensity ratios for detected objects

Ratio	O–CSEs					C–CSEs				
	objects	mean	median	min	max	objects	mean	median	min	max
$\frac{\mathrm{HCN}(1-0)}{\mathrm{CO}(1-0)}$	19	0.10	0.07	0.03[a]	0.49	22	0.68	0.42	0.17	2.2
$\frac{\mathrm{SiO}(2-1)}{\mathrm{CO}(1-0)}$	27	1.1	0.28	0.04	10.1	12	0.078	0.075	0.03	0.17
$\frac{\mathrm{HCN}(1-0)}{\mathrm{SiO}(2-1)}$	19	0.24	0.28	0.04	0.46	12	5.6	6.2	2.3	7.6[b]
$\frac{\mathrm{SO}(3_2-2_1)^{\mathrm{c}}}{\mathrm{CO}(1-0)}$	14	0.086	0.09	0.05[a]	0.13					
$\frac{\mathrm{CS}(2-1)}{\mathrm{CO}(1-0)}$	2	0.029		0.01	0.05	15	0.24	0.25	0.06	0.46
$\frac{\mathrm{SiS}(5-4)}{\mathrm{CO}(1-0)}$	3	0.02		0.004	0.029	7	0.041	0.029	0.01	0.13
$\frac{\mathrm{SiS}(5-4)}{\mathrm{SiO}(2-1)}$	3	0.07		0.02	0.14	7	0.65	0.44	0.25[a]	1.4

[a] There is one upper limit lower than this.
[b] There are lower limits higher than this.
[c] The tentative detection of SO in W Hya is not included in the analysis.

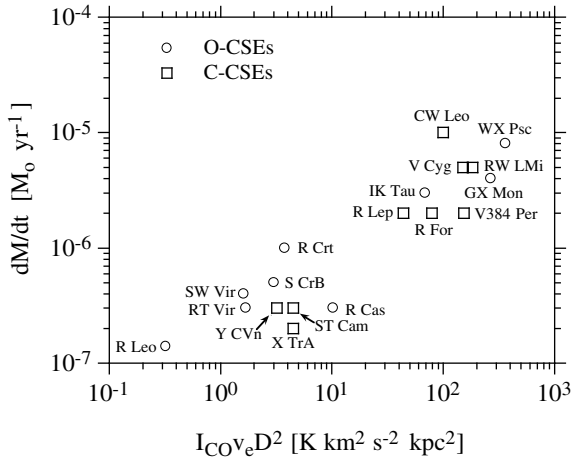

Fig. 2. A comparison between the mass loss rate measure $I_{\rm CO}v_{\rm e}D^2$ and mass loss rate estimates taken from the literature (see text for details)

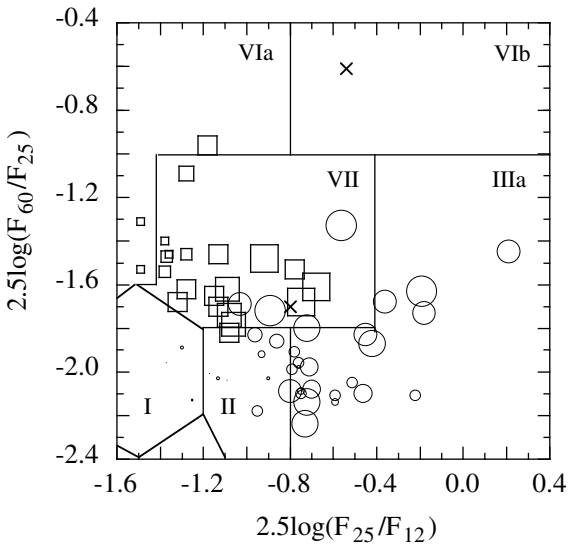

Fig. 3. A plot of the observed stars in a two-colour diagram based on the IRAS–fluxes [the regions introduced by van der Veen & Habing (1988) are also shown]. The area of the symbols (O–CSEs, circles; C–CSEs, squares) are proportional to the mass loss rate measure $I_{\rm CO}v_{\rm e}D^2$. M–stars not detected in CO due to problems with interfering interstellar CO emission are indicated by crosses

to the mass loss rate measure. It is clear that for the M–stars the mass loss rate tends to increase with the [25]/[12]-colour as has been shown by many authors (cf. Bedijn 1987; van der Veen & Rugers 1989), and for the C–stars the high–$\dot{M}$ objects cluster in the area where blackbodies would be found (cf. Olofsson et al. 1993a). There is also a number of high–$\dot{M}$ M–stars in the region where C–stars dominate (VII).

4.2. The HCN/CO line intensity ratio

There is a large difference between the I(HCN,$J = 1\rightarrow0$)/I(CO,$J = 1\rightarrow0$)–distributions for the O– (19 objects) and C–CSEs (22 objects), Fig. 4. The former has a median value of 0.07 and a maximum value of 0.49 (W Hya), while the latter has a median value of 0.42 and a minimum value of 0.17 (07454–7112). The majority of the O–CSEs lies in the narrow range 0.05–0.1. However, there is some overlap in the sense that two out of 19 O–CSEs have ratios above the minimum ratio for the C–CSEs (possibly another two if one takes into account the relative calibration uncertainties). Thus, the $I_{\rm HCN}/I_{\rm CO}$–ratio is not a perfect discriminator between O– and C–CSEs. This result is consistent with the findings of Groenewegen et al. (1996). They found five (probable) C–CSEs with line ratios <0.25 (two of them have a ratio <0.1) using the SEST. Our mean ratios for O– and C–CSEs are 0.10 and 0.68, respectively, i.e., in both cases in excellent agreement with the values obtained by Bujarrabal et al. (1994a), 0.11 and 0.76, respectively. The four S–stars detected in the HCN($J = 1\rightarrow0$) line by Bieging & Latter (1994) have a mean $I_{\rm HCN}/I_{\rm CO}$–ratio of 0.17, i.e, close to the geometrical means of our means (0.27) and medians (0.17) for the O– and C–CSEs.

The reason for the difference in the $I_{\rm HCN}/I_{\rm CO}$–distributions is easily explained. CO is believed to be of photospheric origin in both O– and C–CSEs, and its abundance should roughly equal that of C in the former and O in the latter. i.e., we expect at most a factor of three in difference in the CO abundance between the two types of CSEs. Likewise, HCN is believed to be of photospheric origin in C–CSEs, where its abundance is dependent on the C left-over from the CO formation (a fair fraction of the remaining C is contained in other molecules, e.g., C_2H_2, and dust particles). On the contrary, HCN is believed to be of circumstellar origin in an O–CSE, where it is produced through reactions starting with CH+NO and N+CH_3, where N and CH_x originate from photodissociation of N_2 and CH_4, respectively (Nejad & Millar 1988; Nercessian et al. 1989; Willacy & Millar 1997). Some doubts have been cast upon this scheme since it obviously produces a much higher CN/HCN abundance ratio than is observed (Olofsson et al. 1991; Bachiller et al. 1997), and molecules that should be produced simultaneously with HCN, e.g., CH_3OH and C_2H, are not detected (Charnley & Latter 1997). Millar & Olofsson (1993) explained the detection of H_2CO in OH231.8+4.2 (Lindqvist et al. 1992) using a CH_4-based chemistry, but this object is probably of a very different nature than the ones discussed here.

In Fig. 5 we plot the I(HCN,$J = 1\rightarrow0$)/I(CO,$J = 1\rightarrow0$)–ratios as a function of the mass loss rate measure $I_{\rm CO}v_{\rm e}D^2$. Except for the high value of W Hya (0.49), it appears that this line ratio is essentially independent of the mass loss rate over more than two orders of magnitude for the O–CSEs, the ratio is $0.09\pm0.05\,(1\sigma)$ for $I_{\rm CO}v_{\rm e}D^2 > 0.1$ (which corresponds to roughly $10^{-7}\,{\rm M}_\odot\,{\rm yr}^{-1}$). This behaviour very likely has its roots in the $\dot{M}$-dependences of the number of the CO and HCN molecules and the size of the HCN and CO line–emitting regions. The models predict that the radius of the peak abundance, $R_{\rm p}$, in the HCN–shell of an O–CSE should increase roughly as $\dot{M}^{0.7}$ [ignoring the dependence on $v_{\rm e}$, but $\dot{M}$ substituted with $(\dot{M}/v_{\rm e})$ should give roughly the correct dependence; Nercessian et al. 1989]. It appears that the relative width of the shell, $\Delta R/R_{\rm p}$, decreases with $\dot{M}$, roughly as $\dot{M}^{-0.3}$. The peak abun-

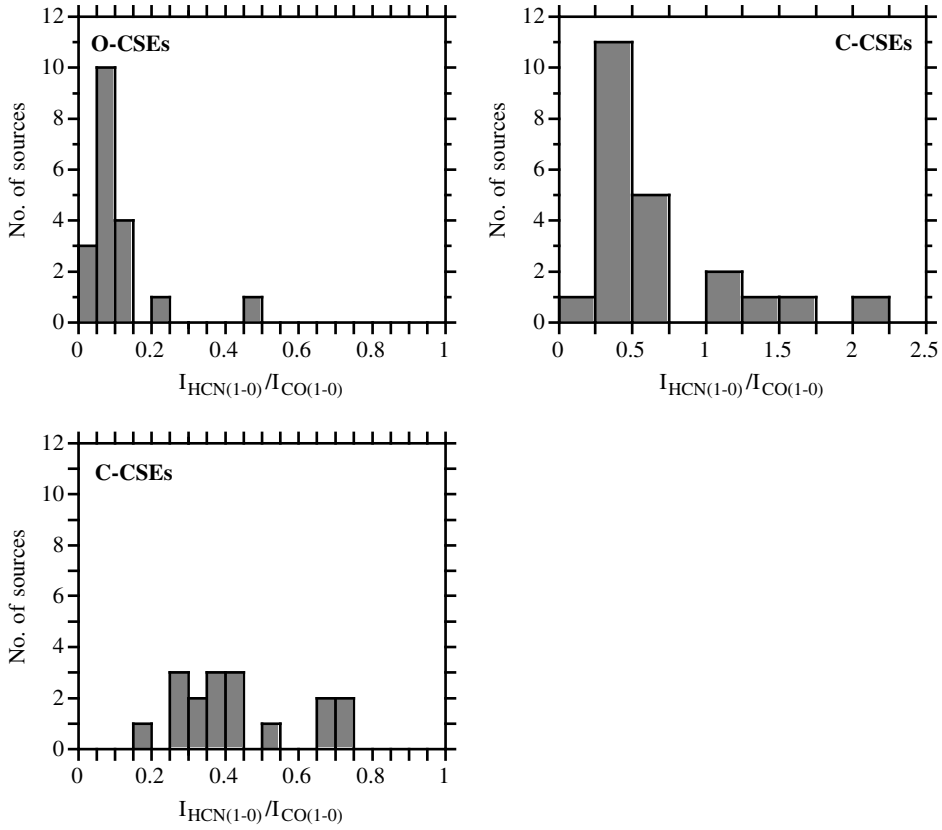

Fig. 4. The I (HCN, $J = 1 \rightarrow 0$) / I(CO, $J = 1 \rightarrow 0$)–distributions for O– and C–CSEs. The distribution of C–CSEs with a line intensity ratio <1 is shown below that of the O–CSEs

dance, on the other hand, seems to be independent of $\dot{M}$ (Nercessian et al. 1989; Willacy & Millar 1997). This implies that the number of HCN molecules in the shell scales roughly as $\dot{M}\Delta R \propto \dot{M}^{1.4}$, and the emitting area (in the form of a disk if one integrates over all velocities) as $R_{\rm p}^2 \propto \dot{M}^{1.4}$. Ignoring possible changes in the excitation with $\dot{M}$, we expect the HCN intensity to scale roughly as $\dot{M}^{1.4}$ (irrespective of the optical depth), i.e., not too different from the $\dot{M}$–dependence of the CO–intensity, $\dot{M}^{1-2}$ (see e.g., Kastner 1992). Thus, the data are in qualitative agreement with what can be expected from theory, but a more detailed analysis, including molecular excitation and radiative transfer, is required to fully explain the observed behaviour. We note that the independence of the HCN/CO line intensity ratio on the mass loss rate is, in principle, also compatible with a photospheric origin of HCN, and the question can only be settled by actually measuring the brightness distributions. Fig. 5 also shows that, except for one (IRC+40004), our upper limits to the HCN intensity for the O–CSEs are not significant, i.e., it is likely that HCN is ubiquitously present in CSEs around M–stars.

In the C–stars the objects with the lowest mass loss rates show surprisingly strong HCN($J = 1 \rightarrow 0$) lines. Three of these stars (W Ori, Y CVn, and X TrA) are known to have time variable, narrow features in this line, indicating the presence of maser action (Olofsson et al. 1993b; Izumiura et al. 1995). This high frequency of ground–state HCN($J = 1 \rightarrow 0$) masers among only the C–stars with the lowest mass loss rates was first noted by Izumiura (1990). The characteristics of the maser emission will be further discussed in Sect. 5. [We note in passing that no strange HCN($J = 1 \rightarrow 0$) line profiles, which would suggest maser emission, have been detected towards O–CSEs, although in many cases the S/N-ratio is too low to warrant such a conclusion.] For the higher mass loss rates the line intensity ratio is essentially independent of the mass loss rate over two orders of magnitude, the ratio is $0.45 \pm 0.27\,(1\sigma)$ for $I_{\rm CO} v_{\rm e} D^2 > 10$ (which corresponds to roughly $> 10^{-6}\,{\rm M}_\odot\,{\rm yr}^{-1}$), although there may be a weak trend of a decrease (see below). Once again, this behaviour is roughly what we expect, even though the origin of HCN is completely different for the C–CSEs (here it is believed to be of photospheric origin). The size of the HCN envelope, determined by photodissociation, scales roughly as $\dot{M}^{0.7}$ (see below), and so the number of HCN molecules increases with $\dot{M}^{1.7}$ (since there is no obvious reason to expect that the HCN abundance depends on $\dot{M}$ for a photosperic species), and the projected area of the HCN envelope increases with $\dot{M}^{1.4}$. Ignoring excitation effects, we expect the HCN intensity to scale roughly as $\dot{M}^{1.4-1.7}$, i.e., within the range of the CO intensity dependence on the mass loss rate.

The possible decline in the $I_{\rm HCN}/I_{\rm CO}$–ratio with mass loss rate for the C–CSEs could be attributed to a change in excitation, e.g., the gradual increasing importance of collisional excitation for HCN in combination with cooler CSEs, and/or a gradual increase in the saturation of the HCN line. The decline is corroborated by the results of Groenewegen et al. (1996). For instance, the five (probable) C–CSEs with HCN/CO intensity ratios below 0.25 have $\dot{M} \approx 5 \times 10^{-6}\,{\rm M}_\odot\,{\rm yr}^{-1}$ (corresponds

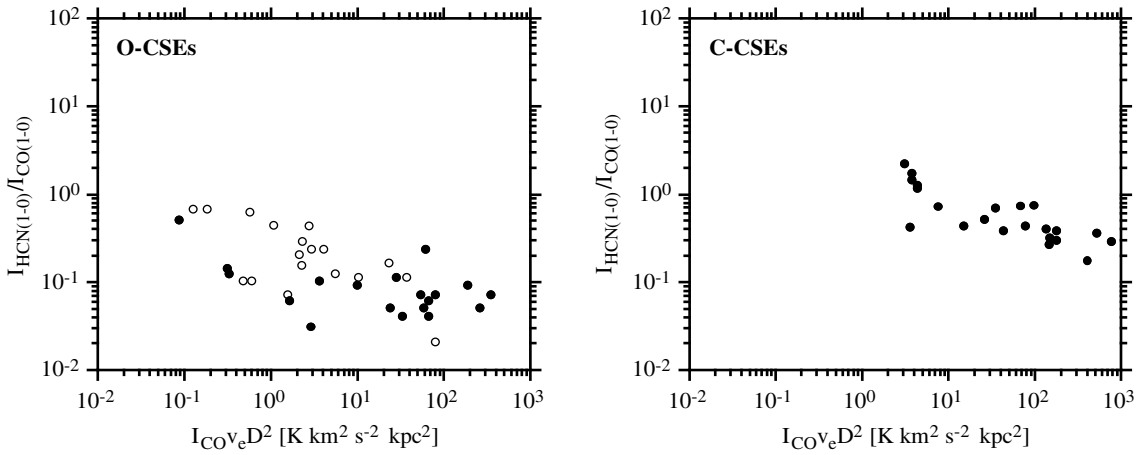

Fig. 5. The $I(\mathrm{HCN},J=1\rightarrow0)/I(\mathrm{CO},J=1\rightarrow0)$–ratio versus the mass loss rate measure $I_{\mathrm{CO}}v_{\mathrm{e}}D^2$ for O– and C–CSEs (open symbols indicate upper limits)

to roughly $I_{\mathrm{CO}}v_{\mathrm{e}}D^2 = 150$). It is conceivable that this intensity ratio increases again for the highest–$\dot{M}$ objects due to the saturation (or even decline) of the CO($J=1\rightarrow0$) intensity at very high mass loss rates (see e.g., Sahai 1990; Kastner 1992). Olofsson et al. (1993b) found a decrease in the estimated HCN abundance with increasing mass loss rate, which they attributed to a systematic underestimate of the mass loss rate (and hence an apparently higher HCN abundance) that gets worse the lower the mass loss rate. It is clear that a more sophisticated model analysis, supplemented with more detailed observational data, is required in order to disentangle the various possible effects.

The argument about the $\dot{M}$–dependence of the size of the emitting region is correct only if $\dot{M}$ is high enough to provide effective dust shielding. Using Eq.(6) of Olofsson et al. (1993b) we find that the photodissociation radius of HCN in a C–CSE can be roughly calculated from the formula (assuming a gas–to–dust mass ratio of 200, and that the dust velocity equals the gas velocity)

$$R_{\mathrm{ph,HCN}} = \frac{v_{\mathrm{e}}}{G_o} + 2.9\times10^{15}\left[\frac{\dot{M}}{10^{-6}\,\mathrm{M_\odot\,yr^{-1}}}\right]^{0.7}\times \times\left[\frac{10\,\mathrm{km\,s^{-1}}}{v_{\mathrm{e}}}\right]^{0.4}\mathrm{cm}, \quad (2)$$

where the unshielded photodissociation rate, G_o, of HCN is $1.1\times10^{-9}\,\mathrm{s^{-1}}$ (van Dishoeck 1988). That is, the mass loss rate has to be higher than $\approx 10^{-7}\,\mathrm{M_\odot\,yr^{-1}}$ (corresponds to $I_{\mathrm{CO}}v_{\mathrm{e}}D^2 \approx 0.3$) for the above discussion to be valid for the C–CSEs. The mass loss rate is well above this value for all our C–stars. Roughly the same line of reasoning can be applied to the O–CSEs where, according to the models, the HCN is produced after the photodissociation of N_2 and CH_4.

4.3. The SiO/CO line intensity ratio

The $I(\mathrm{SiO},J=2\rightarrow1)/I(\mathrm{CO},J=1\rightarrow0)$–distributions of the O– (27 objects) and C–CSEs (12 objects) are shown in Fig. 6. Once again there is a significant difference between the two types of CSEs, but at this time in the opposite direction when compared to the HCN/CO line intensity ratio. The O–CSEs have a median of 0.28, but the mean is as high as 1.1 since there is a considerable spread in the values, from 0.04 (IRC+40004) to 10 (W Hya; not included in the figure). The C–CSEs have a much lower median 0.075, and, in particular, mean 0.078, with a minimum of 0.03 (07454–7112) and a maximum of 0.17 (R Vol). Thus, there is a marked difference in the $I_{\mathrm{SiO}}/I_{\mathrm{CO}}$–ratios of O– and C–CSEs on the average, but it cannot be used to uniquely distinguish between the two. The mean ratios for O– and C–CSEs obtained by Bujarrabal et al. (1994a) are 2.2 and 0.06, respectively, i.e., in good agreement with our results. The five S–stars detected by Bieging & Latter (1994) have a mean $I_{\mathrm{SiO}}/I_{\mathrm{CO}}$–ratio of 0.18, i.e., in between the geometrical means of our means (0.29) and medians (0.14) of the O– and C–CSEs. This, together with the result in Sect. 4.2, indicates that going from a C/O$<$1 to a C/O$\approx$1 chemistry affects to the same extent the HCN and SiO abundances.

As in the HCN/CO case the reason for the difference in the $I_{\mathrm{SiO}}/I_{\mathrm{CO}}$–distributions is easily explained. SiO is believed to be a photospheric species in both O– and C–CSEs, but its dependence on the C/O–ratio is, in a sense, opposite to that of CO, i.e., its abundance is dependent on the left-over O from the CO formation. It is also likely that adsorption onto grains plays an important role for the SiO abundance, and this mechanism may differ in O– and C–CSEs.

The $I(\mathrm{SiO},J=2\rightarrow1)/I(\mathrm{CO},J=1\rightarrow0)$–ratios are shown as a function of the mass loss rate measure, $I_{\mathrm{CO}}v_{\mathrm{e}}D^2$, in Fig. 7. In the O–CSEs the line intensity ratio decreases markedly with the mass loss rate (roughly as $\dot{M}^{-0.7}$), although it is possible that it becomes essentially independent of the mass loss rate for $I_{\mathrm{CO}}v_{\mathrm{e}}D^2 > 10$ (i.e., for $\dot{M} > 10^{-6}\,\mathrm{M_\odot\,yr^{-1}}$), but the scatter is still large. A plot of the SiO line intensity as a function of the CO line intensity shows no correlation between the two. Thus, the data suggest that the SiO line luminosity is relatively insensitive to the mass loss rate (we cannot exclude maser effects also in this ground–state line, but expect that their con-

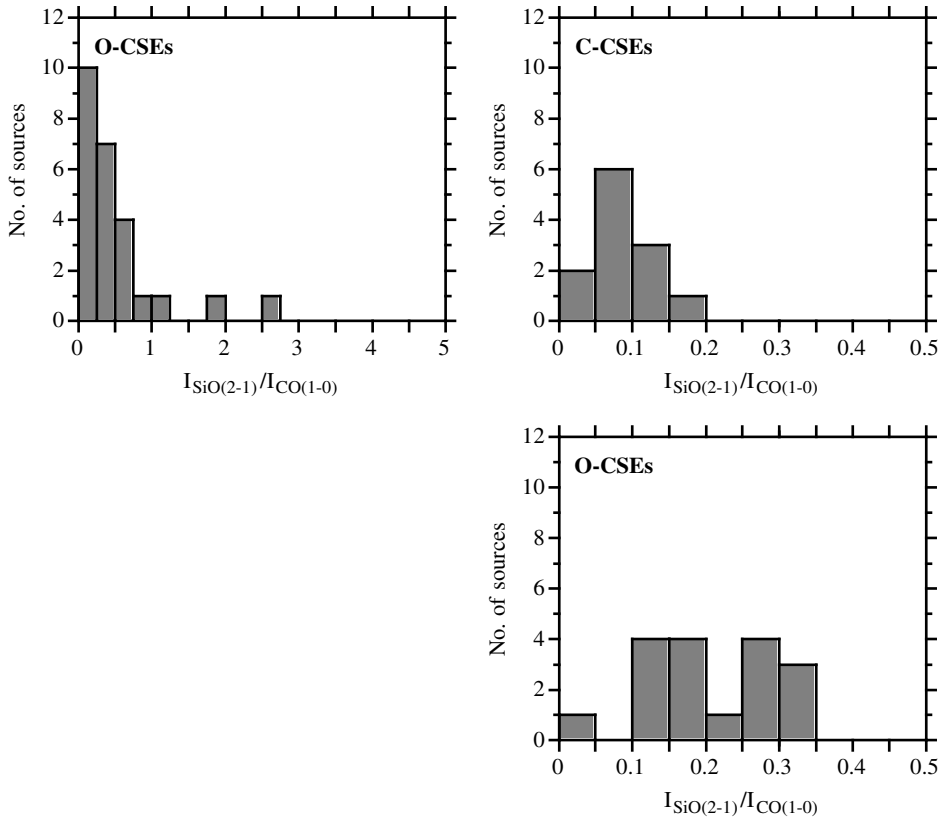

Fig. 6. The $I(\mathrm{SiO}, J = 2 \rightarrow 1)/I(\mathrm{CO}, J = 1 \rightarrow 0)$–distributions for O– (R Hya and W Hya with their line intensity ratios of 6.9 and 10, respectively, are not included in the figure) and C–CSEs. The distribution of O–CSEs with a line intensity ratio <0.5 is shown below that of the C–CSEs

tribution to the line intensity is negligable, see e.g., Nyman & Olofsson 1985). A possible explanation to this is that the radius of the SiO envelope is determined by grain adhesion, which increases with density, rather than photodissociation, which decreases with density (cf. Sahai & Bieging 1993). This can be checked by comparing the linear sizes [half–maximum intensity angular sizes from Lucas et al. (1992), assuming exponential brightness distributions, scaled to the distances used in this paper] of the SiO line–emitting regions of six of the stars in our sample (WX Psc, IK Tau, R Leo, W Hya, RX Boo, and R Cas) with the mass loss rate measure. The result is a very good correlation between the two, but the depencence on the mass loss rate measure is much weaker than that of for instance the HCN shell radius [the exponent is $\approx$0.3, while for HCN the results of Nercessian et al. (1989) and Eq. (1) point to an exponent $\approx$0.5, a result in accordance with recent interferometer observations of Lindqvist et al. (priv. com.)]. However, as pointed out by Sahai & Bieging (1993) the angular sizes measured by Lucas et al. (1992) are surprisingly similar for all stars, suggesting that the brightness distributions rather follow a scale–free power-law. If so, the correlation found is merely an effect of the different distances to the sources. Possibly, the SiO excitation dependence on the mass loss rate is of such a character that combined with other effects the SiO intensity becomes essentially independent of the mass loss rate.

It is difficult to establish whether or not there is any trend for the C–CSEs since only the higher–$\dot{M}$ objects are detected, and the upper limits for the low–$\dot{M}$ are not significant in comparison with these. We note here the peculiar line profile of the SiO($J = 2 \rightarrow 1$) line towards R Lep, which may indicate the presence of maser emission in this line (see Fig. 1). Similar, weak, and time variable features have been seen towards O–CSEs (Nyman & Olofsson 1985).

4.4. The HCN/SiO line intensity ratio

The line intensity ratios discussed in the two previous sections suggest that the $I_{\mathrm{HCN}}/I_{\mathrm{SiO}}$–ratio should be a very good discriminator between O– and C–CSEs, since the HCN and SiO intensities show opposite trends with the C/O–ratio. Indeed, our data show a significant difference between the $I(\mathrm{HCN}, J = 1 \rightarrow 0)/I(\mathrm{SiO}, J = 2 \rightarrow 1)$–distributions of the O– (19 objects) and C–CSEs (12 objects), Fig. 8. The former has a median value of 0.28 and a maximum value of 0.46, while the latter has a median value of 6.2 and a minimum value of 2.3 (note also that none of the lower limits is lower than this), i.e, the lowest C–CSE ratio is well above (by a factor of 5) the highest O–CSE ratio, and the medians differ by a factor of 20. The difference is so large, compared to the uncertainties in the line intensity ratios of the high–ratio O–CSEs and the low–ratio C–CSEs (estimated to be less than 30%), that one can safely use this line intensity ratio to distinguish between "normal" O– and C–CSEs. This result is in perfect agreement with that obtained by Bujarrabal et al. (1994a,b). Their mean ratios for O– and C–CSEs are 0.28 and 12.5. respectively, while we find 0.24 and 5.6, respectively. The difference for the C–CSEs is due to a few objects in the Bujarrabal et al. sample that have very high $I_{\mathrm{HCN}}/I_{\mathrm{SiO}}$–ratios. The four S–stars detected in the HCN($J = 1 \rightarrow 0$) and SiO($J =$

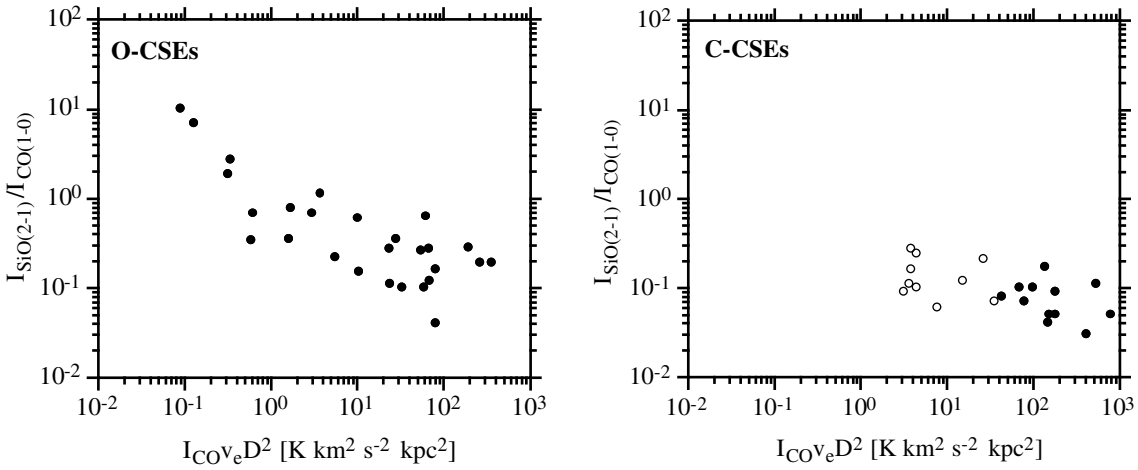

Fig. 7. The $I(\mathrm{SiO},J=2\rightarrow1)/I(\mathrm{CO},J=1\rightarrow0)$–ratio versus the mass loss rate measure $I_{\mathrm{CO}}v_{\mathrm{e}}D^2$ for O– and C–CSEs (open symbols indicate upper limits)

$2\rightarrow1$) lines by Bieging & Latter (1994) have a mean line intensity ratio of 1.16, i.e., a value close to the geometrical means of our means (1.16) and medians (1.32) for the O– and C–CSEs, and all the individual ratios lie above our maximum ratio for the O–CSEs and below our minimum ratio for the C–CSEs.

The HCN/SiO line intensity ratio for the O–CSEs shows a pronounced positive dependence on the mass loss rate measure, roughly as $(I_{\mathrm{CO}}v_{\mathrm{e}}D^2)^{0.3}$ (we discuss below the possibility of a bimodal distribution), Fig. 9. The dependence on mass loss rate of the HCN intensity and the corresponding (in comparison) indepence of the SiO intensity is the reason for this behaviour. The behaviour is quite different for the C–CSEs, where this ratio appears to have no dependence on the mass loss rate (however, note that this applies to a mass loss rate range where also the O–CSEs show little dependence), but it is difficult to draw any definite conclusions since only the stars with the higher mass loss rates have SiO lines that are strong enough to detect.

The $I(\mathrm{HCN},J=1\rightarrow0)/I(\mathrm{SiO},J=2\rightarrow1)$–distribution of the O–CSEs appears to be bimodal, Fig. 8. Roughly half of the stars have a ratio of $\approx$0.35, while the rest have ratios $<$0.1. The reason for this could be the $\dot{M}$–dependence of the line intensity ratio, combined with the fact that there are relatively few sources in the range $5 < I_{\mathrm{CO}}v_{\mathrm{e}}D^2 < 50$. However, it cannot be excluded that the stars with $I_{\mathrm{CO}}v_{\mathrm{e}}D^2 < 10$ have a relatively constant and low $I_{\mathrm{HCN}}/I_{\mathrm{SiO}}$–ratio, and that those with $I_{\mathrm{CO}}v_{\mathrm{e}}D^2 > 10$ also have a relatively constant, but distinctly, higher line intensity ratio. There is no obvious reason for such a bimodality.

Lindqvist et al. (1992) found that the HCN detection probability increased with the [60]/[25]-colour, and they speculated that this could possibly be due to an increase in the abundance of C. It is clear from Fig. 3 that some of the O–CSEs have [60]/[25]-colours that fall in the same range as the C–CSEs, and an increase in the C/O–ratio will almost certainly lead to an increase in the circumstellar HCN abundance and a decrease in the photospheric SiO abundance. However, our larger sample shows that the detection probability is mainly determined by the mass loss rate. In particular, high–$\dot{M}$ O–CSEs with a low [60]/[25]-colour also have a high $I_{\mathrm{HCN}}/I_{\mathrm{SiO}}$–ratio. Thus, there is nothing in our data that indicates that the O–CSEs have a spread in the C/O–ratio.

4.5. The SO/CO line intensity ratio

The $I(\mathrm{SO},J_K=3_2\rightarrow2_1)/I(\mathrm{CO},J=1\rightarrow0)$–distribution for O–CSEs (14 objects) is presented in Fig. 10 (the tentative detection of SO in W Hya is not included in the analysis). The median value is 0.09, and the mean ratio is $0.086\pm0.025\,(1\sigma)$. Apparently, the SO/CO intensity ratio falls in a narrow range [except for IRC–30398 our upper limits to the SO($J_K=3_2\rightarrow2_1$) emission are not significant, see Fig. 11], and we can expect that SO is abundant in the majority of all O–CSEs. This result suggests that the SO intensity scales with the mass loss rate in the same way as the CO intensity does. Fig. 11 clearly shows that this is also the case. There are two main routes for the production of circumstellar SO, S+OH $\rightarrow$ SO+H and O+SH $\rightarrow$ SO+H (Scalo & Slavsky 1980; Nejad & Millar 1988; Willacy & Millar 1997). In both cases the production is dependent on the formation of OH through the photodissociation of H_2O, since in the latter reaction the free O is produced from the photodissociation of H_2O and OH. The free S is probably in the form of H_2S initially. SO is effectively destroyed in the reaction SO+OH $\rightarrow$ SO_2+H. Thus, irrespective of the dominant reaction we expect the size of the SO–shell to be dependent on the mass loss rate in roughly the same way as the OH–shell. According to Netzer & Knapp (1987) the radius of the OH–shell scales as $\dot{M}^{0.7}$ (for $\dot{M} > 5\times10^{-7}\,\mathrm{M}_\odot\,\mathrm{yr}^{-1}$), i.e., in the same way as the radius of the HCN–shell (see Sect. 4.2). According to the results of Nejad & Millar (1988) the peak SO abundance is only marginally dependent on the mass loss rate (as is that of HCN), and consequently we expect the SO/CO and HCN/CO line intensity ratios to behave in a similar manner. It appears, in fact, that the SO intensity correlates significantly better with the CO intensity than does the HCN with CO, compare Figs 5 and 11. The reason for the apparently tighter relation between

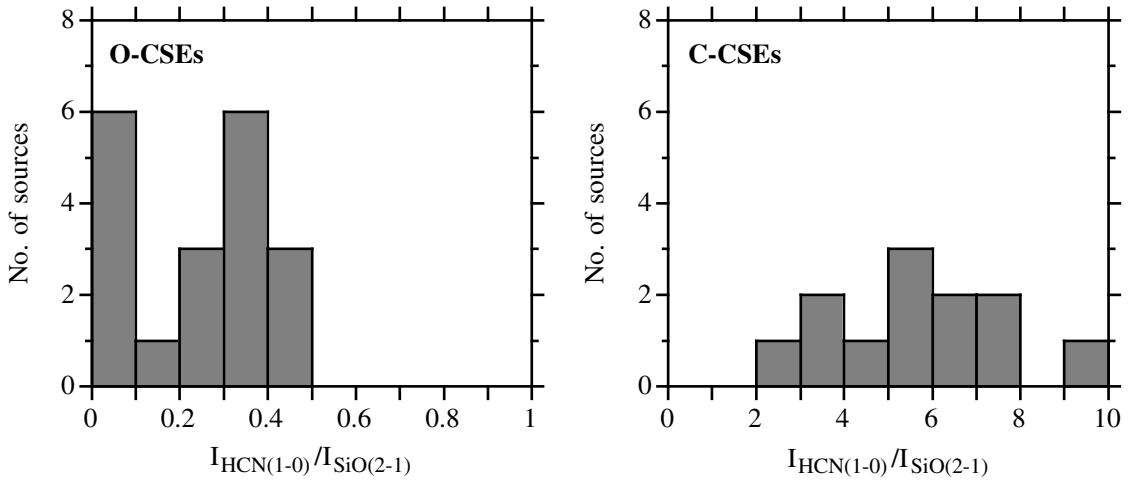

Fig. 8. The $I(\mathrm{HCN},J=1\rightarrow0)/I(\mathrm{SiO},J=2\rightarrow1)$–distributions for O– and C–CSEs

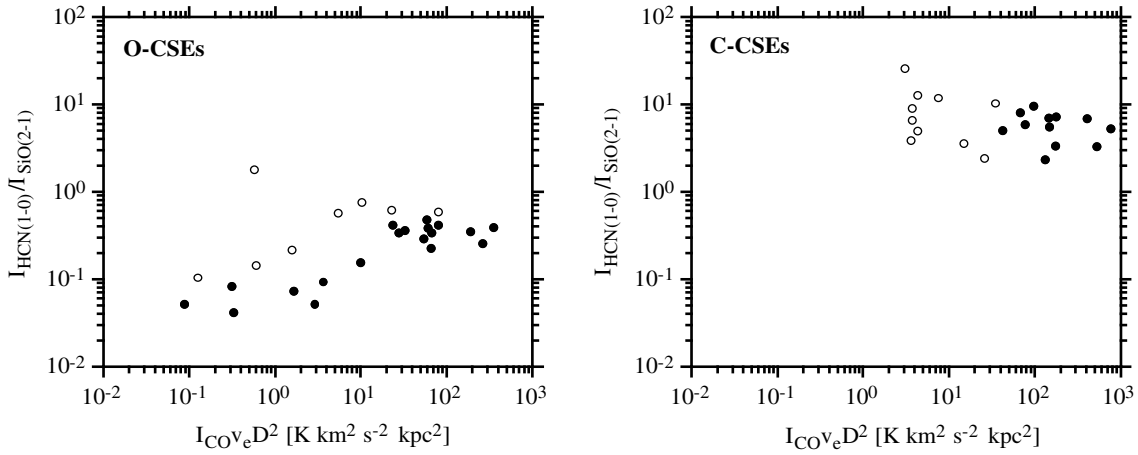

Fig. 9. The $I(\mathrm{HCN},J=1\rightarrow0)/I(\mathrm{SiO},J=2\rightarrow1)$–ratio versus the mass loss rate measure $I_{\mathrm{CO}}v_{\mathrm{e}}D^2$ for O– and C–CSEs (open symbols indicate upper limits for O–CSEs and lower limits for C–CSEs)

the SO and CO intensities is not clear, but it can be due to both chemistry and excitation. The former very likely plays a role since the SO abundance is dependent on the H_2O abundance, while the HCN abundance is dependent on the abundance of the free C (due to photodissociation of CH_4, which in itself has to be produced in the inner CSE according to the models), which presumably can vary substantially. Also, the outer radius of the HCN–shell is determined by photodissociation, while the outer radius of the SO–shell depends on the chemical destruction (see above).

We have not attempted to detect SO towards C–CSEs. Bujarrabal et al. (1994a) failed to do so despite a relatively sensitive search towards a few objects.

We have not detected the higher-lying (in energy), but inherently weaker, $\mathrm{SO}(J_K=2_2\rightarrow1_1)$ line (the 3_2 and 2_2 levels have energies of 9.2 and 19.3 K, respectively). SO has a $^3\Sigma$ ground state, and the rotational energy levels can be divided into three groups ($J=N-1$, $J=N$, and $J=N+1$, where J and N are the total and rotational angular momentum quantum numbers in the pure Hund's coupling case b, respectively). Radiative transitions between the groups are very weak compared to transitions within the groups (except for the lower J-values), and we therefore expect the excitation between the groups to be largely determined by collisions. The upper limits to the $\mathrm{SO}(2_2\rightarrow1_1)$ line are low and indicate a kinetic temperature below 20 K in the SO line–emitting region.

4.6. Line intensity ratios involving CS and SiS

The detections of CS and SiS in O–CSEs are so few that we will only briefly discuss the most interesting line intensity ratios involving these species. We have detected only two O–CSEs in CS (three more O–CSEs of AGB–stars have been detected in CS: WX Psc, RX Boo, and IRC–10529, Bujarrabal et al. 1994a), and only three O–CSEs in SiS (one more O–CSE has been detected in SiS: IRC–10529, Bujarrabal et al. 1994a). It is obvious that only tentative conclusions can be drawn from these data. We present the results as $I(\mathrm{CS},J=2\rightarrow1)/I(\mathrm{CO},J=1\rightarrow0)$–, $I(\mathrm{SiS},J=5\rightarrow4)/I(\mathrm{CO},J=1\rightarrow0)$–, and $I(\mathrm{SiS},J=$

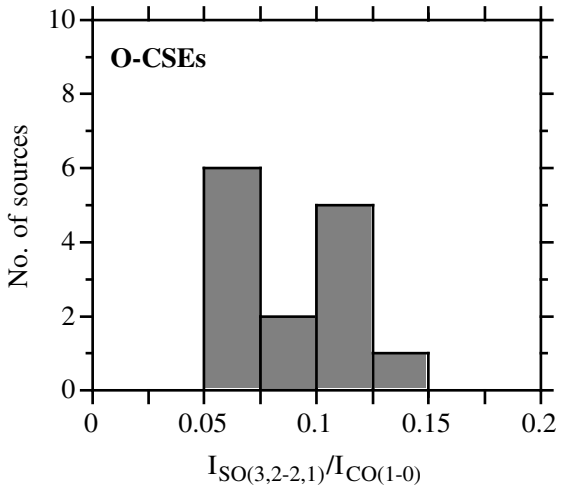

Fig. 10. The $I(\mathrm{SO},J_K = 3_2 \rightarrow 2_1)/I(\mathrm{CO},J = 1 \rightarrow 0)$–distribution for O–CSEs

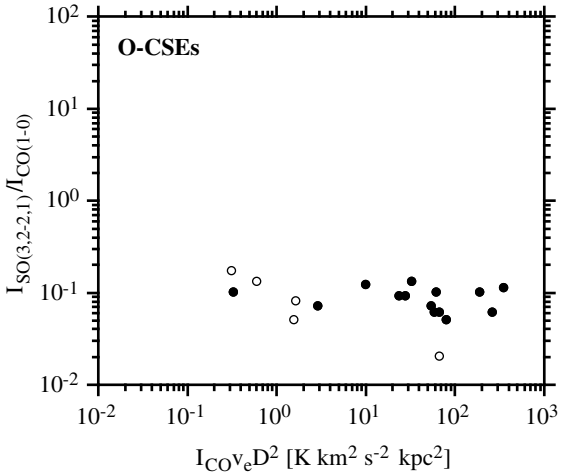

Fig. 11. The $I(\mathrm{SO},J_K = 3_2 \rightarrow 2_1)/I(\mathrm{CO},J = 1 \rightarrow 0)$–ratio versus the mass loss rate measure $I_{\mathrm{CO}} v_{\mathrm{e}} D^2$ for O–CSEs (open symbols indicate upper limits)

$5 \rightarrow 4)/I(\mathrm{SiO},J = 2 \rightarrow 1)$–distributions for the O– and C–CSEs in Figs 12, 13, and 14. The upper limits for the O–CSEs are not significant.

The mean $I(\mathrm{CS},J = 2 \rightarrow 1)/I(\mathrm{CO},J = 1 \rightarrow 0)$–ratio of the O–CSEs, 0.029, is much lower than that of the C–CSEs, 0.24. However, it is clear already from this limited data set that this line intensity ratio does not provide a clear discrimination between O– and C–CSEs, since there is a pronounced tail of low ratios for the C–CSEs. The difference in the $I_{\mathrm{CS}}/I_{\mathrm{CO}}$–distributions is expected also from theory. In an O–CSE the CS molecules are produced in the envelope via the reactions starting with C^++H_2S or S^++CH leading to the formation of HCS^+, which dissociatively recombines with an electron or proton transfers with NH_3, or via the reactions C+SO → CS+O and C+SH → CS+H (Nejad & Millar 1988; Willacy & Millar 1997). The predicted abundances (few $\times\ 10^{-7}$) are in all cases much lower than the expected CS abundance in a C–CSE. In the latter case the observed CS is believed to be of photospheric origin, and Olofsson et al. (1993a) derived a maximum abundance of $\approx 3 \times 10^{-5}$. However, the photospheric CS abundance is rather sensitive to temperature (and to some extent the C/O–ratio) and abundances as low as $\approx 10^{-8}$ are possible. This probably explains the tail toward low $I_{\mathrm{CS}}/I_{\mathrm{CO}}$–ratios for the C–CSEs.

The mean $I(\mathrm{SiS},J = 5 \rightarrow 4)/I(\mathrm{CO},J = 1 \rightarrow 0)$–ratio of the O–CSEs, 0.02, is lower than that of the C–CSEs, 0.041 (note that this value applies to relatively high–$\dot{M}$ objects), but even this limited data set shows that this line intensity ratio can not be used as a discriminator. In an O–CSE the SiS is probably a photospheric species [and possibly additionally produced in the envelope through the reaction S^++SiH → SiS+H^+ if grain depletion of Si is negligable, Scalo & Slavsky (1980)], and the calculated SiS/SiO abundance ratio is ≈0.1 (Tsuji 1973). In a C–CSE the SiS is also believed to be of photospheric origin, and its predicted abundance ($\leq 3 \times 10^{-5}$) is relatively insensitive to temperature and C/O-ratio (Olofsson et al. 1993b). The calculated SiS/SiO abundance ratios is $\gtrsim$1 in this case. Thus, considering that the SiO/CO line intensity ratio is 5–10 times higher in O–CSEs than in C–CSEs, the small difference in the $I_{\mathrm{SiS}}/I_{\mathrm{CO}}$–distributions is not unexpected.

The mean $I(\mathrm{SiS},J = 5 \rightarrow 4)/I(\mathrm{SiO},J = 2 \rightarrow 1)$–ratio of the C–CSEs is about 10 times higher than that of the O–CSEs, i.e., the average line intensity ratio difference agrees with the expected abundance ratio difference. Despite this, this line intensity ratio is not a perfect discriminator since, for unknown reason, some C–CSEs are very weak in the SiS($J = 5 \rightarrow 4$) line. The C–CSEs are divided into a low– and a high–ratio group, but this could be an effect of too poor statistics.

Line intensity ratios of further interest to compare are CS/HCN, CS/SiS, and CS/SO. CS and HCN have the same origins in O– and C–CSEs, but they differ between the two chemistries, i.e., they are circumstellar in O–CSEs and photospheric in C–CSEs. The mean $I(\mathrm{CS},J = 2 \rightarrow 1)/I(\mathrm{HCN},J = 1 \rightarrow 0)$–ratio is 0.17 in O–CSEs, while for the C–CSEs the ratios centre around ≈0.6, but with a substantial tail towards values lower than 0.1. The mean $I(\mathrm{CS},J = 2 \rightarrow 1)/I(\mathrm{SiS},J = 5 \rightarrow 4)$–ratios are 1.7 and 10 in O– and C–CSEs, respectively. None of these line intensity ratios are likely to be good discriminators between O– and C–CSEs. The mean $I(\mathrm{CS},J = 2 \rightarrow 1)/I(\mathrm{SO},J_K = 3_2 \rightarrow 2_1)$–ratio in O–CSEs is 0.3.

4.7. Anomalous line intensity ratios and peculiar sources

The results based on line intensity ratios presented in the previous sections apply only to "normal" CSEs. By "normal" in this context we mean a CSE formed by a relatively constant mass loss rate (both in magnitude and chemical composition) over a period longer than the time required to substantially change the density structure or the composition of the gas within the line emitting regions, $\lesssim 10^3$ years, i.e., on intermediate time scales. A rapid change in the chemical composition of the ejected gas or in the mass loss rate would eventually lead to anomalous line intensity ratios. In the former case, we expect the CSE to show a chemistry different from that expected from the chemical composition of

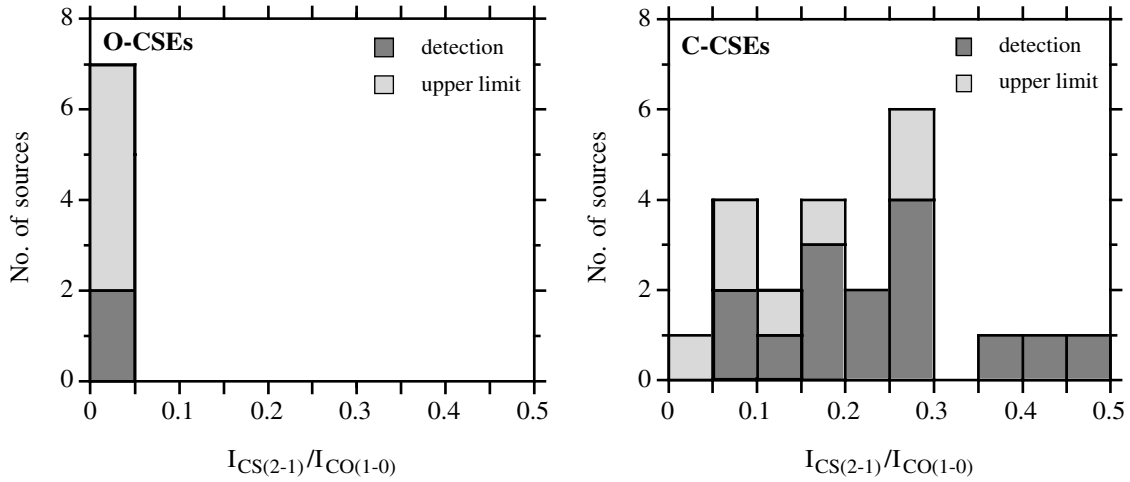

Fig. 12. The $I(\mathrm{CS}, J = 2 \rightarrow 1)/I(\mathrm{CO}, J = 1 \rightarrow 0)$–distributions for O– and C–CSEs

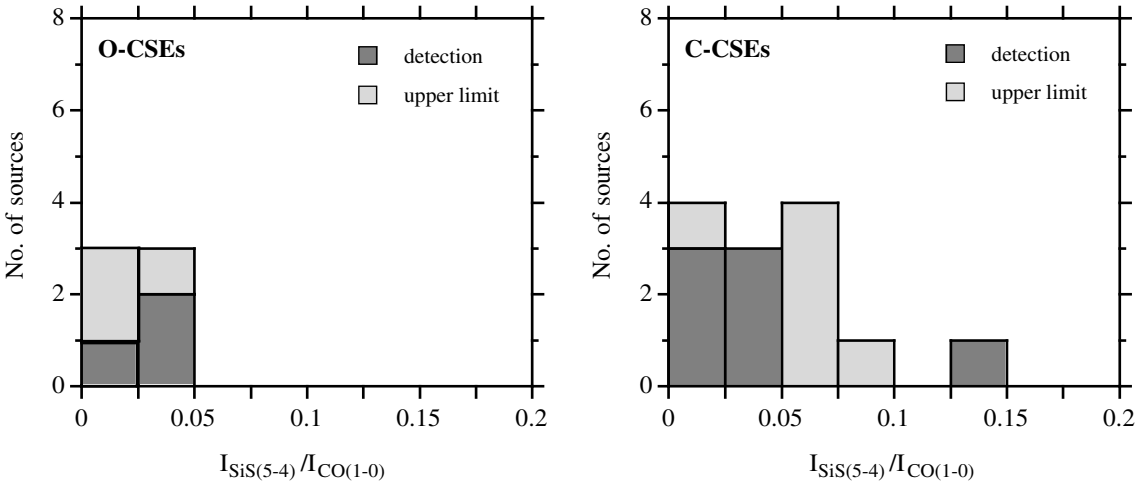

Fig. 13. The $I(\mathrm{SiS}, J = 5 \rightarrow 4)/I(\mathrm{CO}, J = 1 \rightarrow 0)$–distributions for O– and C–CSEs

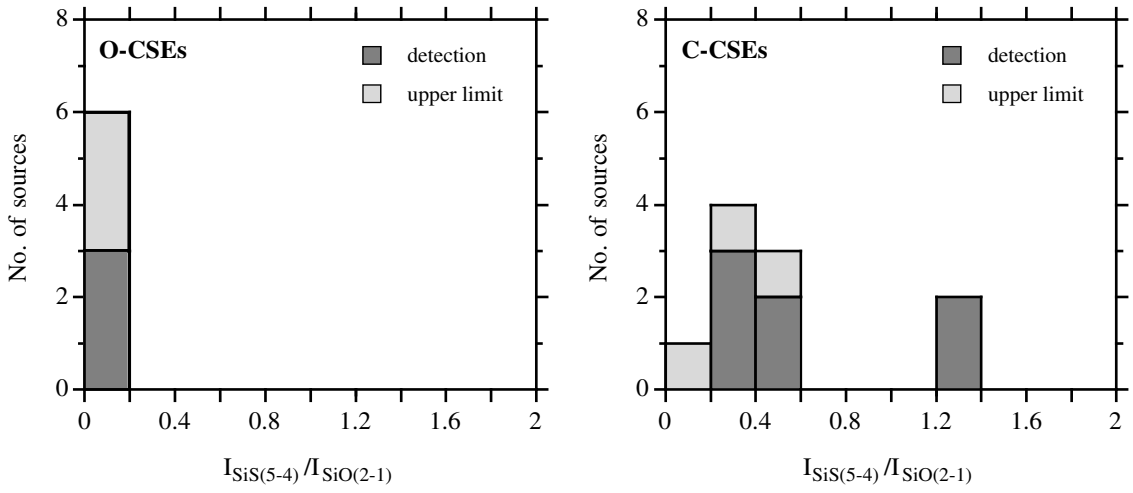

Fig. 14. The $I(\mathrm{SiS}, J = 5 \rightarrow 4)/I(\mathrm{SiO}, J = 2 \rightarrow 1)$–distributions for O– and C–CSEs

the central star. We find no evidence for such a situation in any of the objects observed, e.g., a high (low) $I_{\rm HCN}/I_{\rm SiO}$–ratio in a CSE around an M–star (C–star). In the latter case, the emission from molecular species excited at different radii may behave differently, e.g., a recent decrease in the mass loss rate decreases the emission from molecules excited close to the star while the CO emission is hardly affected. Interesting examples of this are provided by the carbon star R Scl, which, due to a probably recently detached CSE, shows a low I(HCN,$J = 1 \rightarrow 0$)/I(CO,$J = 1 \rightarrow 0$)–ratio and a high I(CN,$N = 1 \rightarrow 0$)/I(HCN,$J = 1 \rightarrow 0$)–ratio, and the carbon stars U Ant, S Sct, and TT Cyg with clearly detached shells, which show very low upper limits to a number of I(X,$j \rightarrow i$)/I(CO,$J = 1 \rightarrow 0$)–ratios (Bujarrabal & Cernicharo 1994; Olofsson et al. 1996). Once again, we find no line intensity ratios that indicate significant mass loss rate variations on intermediate time scales for our objects.

However, there is one source in our sample with an apparently non–normal CSE [the C–star U Cam appears to have a detached shell (Lindqvist et al. 1996)], which despite this exhibits no obviously anomalous line intensity ratios. This shows that line intensity ratios do not unambiguously identify CSEs with non–normal characteristics. Furthermore, the M–star W Hya shows a high I(HCN,$J = 1 \rightarrow 0$)/I(CO,$J = 1 \rightarrow 0$)–ratio, and, in particular, a very high I(SiO,$J = 2 \rightarrow 1$)/I(CO,$J = 1 \rightarrow 0$)–ratio compared to the other M–stars [the latter ratio is high also for R Dor and R Hya]. We have no obvious explanation of this.

5. HCN($J = 1 \rightarrow 0$) masers in C–CSEs

The existence of strong HCN masers associated with carbon stars was discovered accidentally when searching for HCO^+($J = 1 \rightarrow 0$) emission towards C–CSEs (Guilloteau et al. 1987). The masing $J = 1 \rightarrow 0$ transition lies in the vibrationally excited state (0,2^0,0) about 2050 K above the ground state. Lucas et al. (1988) showed that this maser is not uncommon, but it appears to be restricted to a limited mass loss rate range ($\approx 10^{-6} - 10^{-5}\,{\rm M}_\odot\,{\rm yr}^{-1}$). Subsequently, Lucas & Cernicharo (1989) detected another strong HCN maser. In this case it was the $J = 2 \rightarrow 1$ transition in the vibrationally excited state (0,1^{1_c},0). In IRC+10216, the archetype of C–CSEs, they also observed all possible $J = 1 \rightarrow 0$, $2 \rightarrow 1$, and $3 \rightarrow 2$ transitions in the fundamental and two lowest–lying vibrational states of HCN, and inferred that a pump mechanism similar to that of the strong SiO masers associated with M–stars is quite possible.

The presence of ground–state $J = 1 \rightarrow 0$ maser emission was first noticed by Izumiura et al. (1987) [see also Izumiura (1990) and Olofsson et al. (1993b)]. The maser emission nature is inferred from the presence of time–variable narrow features. It appears not to be a question of strong masers, but it makes the estimate of the HCN abundance uncertain, and it adds further evidence that the excitation of circumstellar HCN is quite complicated. The vibrationally excited strong masers almost certainly lie very close to the star (Carlstrom et al. 1990; Lucas & Guilloteau 1992). For the ground–state masers the situation is unclear. We have therefore performed a time monitoring study of the HCN($J = 1 \rightarrow 0$) emission from two bright carbon stars, W Ori (semiregular variable, P≈210 days) and X TrA (irregular variable). The spectra are presented in Fig. 15. The total integrated fluxes of the two sources vary irregularly with time at levels that are not significant when the calibration uncertainty is taken into account. For both sources the line consists of two components: a broad emission which covers roughly the same velocity range as the CO($1 \rightarrow 0$) emission [data from Olofsson et al. (1993a)], and narrow features that predominantly appear at the blue– and redshifted edges of the emission. The redshifted feature lies somewhat closer to the systemic velocity than the, more rarely occurring, blueshifted feature, and it is in general stronger, a conclusion also reached by Izumiura et al. (1995) for W Ori and Y CVn (a J–type carbon star).

The CN observations of Bachiller et al. (1997) show anomalous I(CN,$N = 2 \rightarrow 1$)/I(HCN,$J = 1 \rightarrow 0$)–ratios for W Ori, UU Aur, and Y CVn, further emphasizing the possible importance of maser action in the HCN($J = 1 \rightarrow 0$) line. However, the situation appears even more complicated since a comparison of CN($N = 1 \rightarrow 0$) and CN($N = 2 \rightarrow 1$) intensities suggests maser action in the CN($N = 2 \rightarrow 1$) line in W Ori and UU Aur.

The interpretation of the HCN($J = 1 \rightarrow 0$) data is made difficult by the hyperfine structure of the J=1 level, which results in three lines that are shifted in velocity with respect to each other by an amount that is usually lower than the expansion velocity of the CSE. Hence, the line profile consists of three blended lines, see Fig. 15, and the radiative transfer becomes complicated (Truong–Bach & Nguyen–Q–Rieu 1989).

We find comparatively very little HCN($J = 1 \rightarrow 0$) emission outside the velocity range of the CO emission for both stars (on average $\lesssim$10% of the total intensity), showing that the approaching (receding) material emits very little in the $F = 0 \rightarrow 1$ ($F = 1 \rightarrow 1$) transition. This indicates that the emission is dominated by the $F = 2 \rightarrow 1$ line. Furthermore, the strong redshifted feature cannot be due to the $F = 0 \rightarrow 1$ component (assuming that no gas with velocities outside the CO range exists). Likewise, the blueshifted feature that occasionally appears cannot be due to the $F = 1 \rightarrow 1$ component. On the other hand, the red– and blueshifted features can be due to gas at roughly the systemic velocity emitting in the $F = 1 \rightarrow 1$ and $F = 0 \rightarrow 1$ component, respectively. The red- and blueshifted features can equally well be due to receding and approaching gas emitting in the $F = 2 \rightarrow 1$ line, i.e., a structure similar to that of an OH 1612 MHz maser, although the symmetry around the systemic velocity is not perfect here. The $F = 1 \rightarrow 1$ emission goes unaffected through the envelope. The redshifted part of the $F = 2 \rightarrow 1$ emission can be absorbed or amplified in the $F = 1 \rightarrow 1$ transition, and if the latter is inverted this may cause a strong maser feature that appear somewhere at intermediate redshifted velocities. The blueshifted $F = 2 \rightarrow 1$ emission is unaffected, and if there is radial amplification the blue maser feature should appear at the blueshifted edge of the CO emission. The same thing happens to the $F = 0 \rightarrow 1$ emission except that it becomes affected also by the $F = 2 \rightarrow 1$ transition. This discussion suggests that the most reasonable explanation to the data, although by no means unique, is radial amplification in the $F = 2 \rightarrow 1$ line, and the redshifted feature may be further amplified and

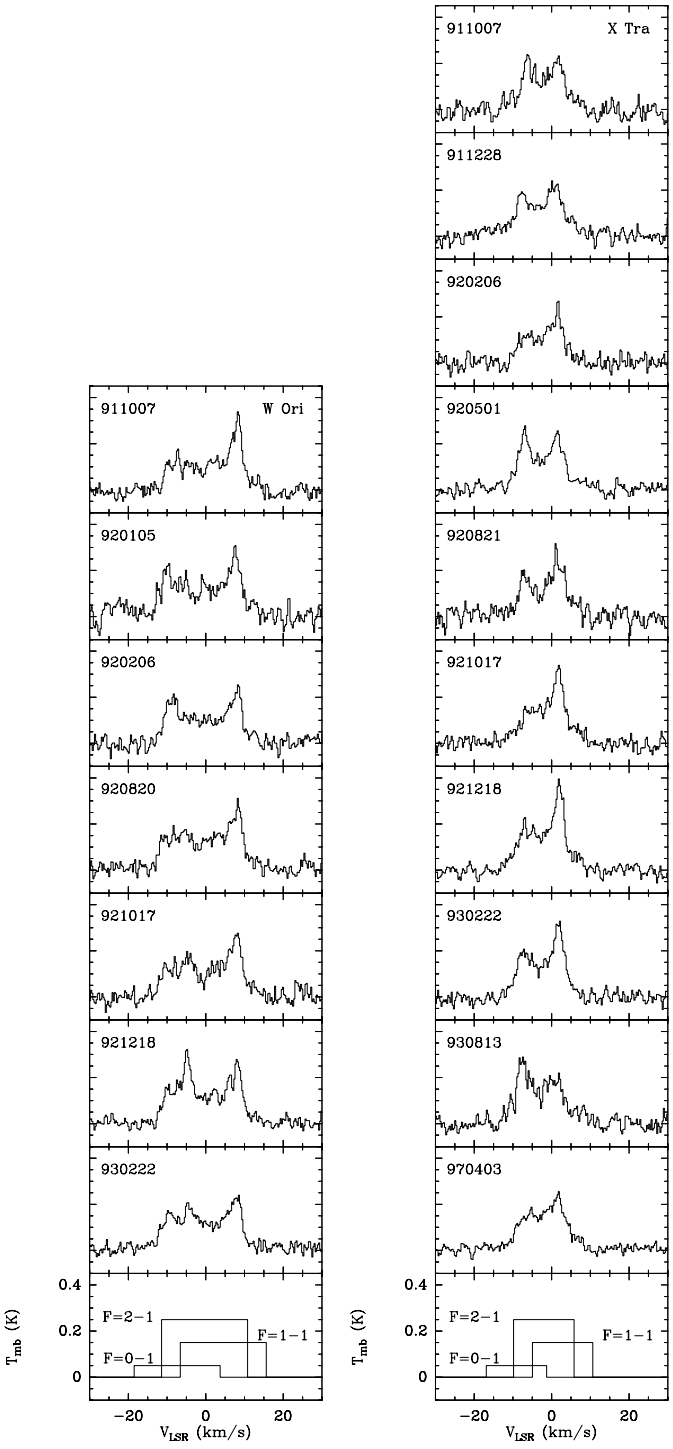

Fig. 15. HCN($J = 1 \rightarrow 0$) spectra of the two bright carbon stars W Ori and X TrA (the datum of the observation is shown in the panel). The hyperfine structure of the line is shown for each source [centre and expansion velocities are taken from Olofsson et al. (1993a)]. The $F = 0 \rightarrow 1$ and $F = 1 \rightarrow 1$ transitions are shifted by -7.1 and +4.8 km s^{-1}, respectively, with respect to the $F = 2 \rightarrow 1$ transition, and their LTE strengths are 1:3:5

shifted to lower velocities by the $F = 1 \rightarrow 1$ transition. An indication that the $F = 1 \rightarrow 1$ transition may play a role is given by the Dec.–92 and Febr.–93 W Ori spectra where a narrow feature at intermediate velocities could be due to radial amplification in the $F = 1 \rightarrow 1$ line in the approaching gas.

The sharp decline in maser intensity at a mass loss rate of $\approx 5 \times 10^{-7}\,M_\odot\,\mathrm{yr}^{-1}$ (see Fig. 5) suggests that there is a clear change in the conditions necessary for maser emission rather than a concealing of the maser emission by an even more intense thermal emission from the whole CSE. The abruptness indicates that the change has something to do with the conditions closer to the star (e.g., the mass loss mechanism), rather than a change over the entire CSE (e.g., due to optical depth effects in the excitation), which is expected to result in a more gradual transition to non–masing emission. Apparently, the conditions in O–CSEs, or perhaps the HCN abundance, are not favourable to maser emission. This is not unexpected since if the models are correct there are no HCN molecules in the inner region of an O–CSE.

6. Conclusions

We have utilized molecular line intensity ratios in a study of 39 and 22 CSEs around M– and C–stars, respectively. Our conclusions are:

1) There is nothing in the data that contradicts that for our sample the CSEs have the same basic chemistry (i.e., C/O$<$1 or $>$1) as the central stars.

2) There is nothing in the data that contradicts that for our sample the stellar mass loss rates have been relatively constant over the last $\lesssim 10^3$ years.

3) SO and the C–bearing species HCN are ubiquitous in O–CSEs, and they are produced in quantities qualitatively consistent with a photo–induced circumstellar chemistry.

4) The HCN($J = 1 \rightarrow 0$)/SiO($J = 2 \rightarrow 1$) intensity ratio discriminates uniquely between "normal" O– and C–CSEs. Considering also the strength of the various circumstellar molecular lines it is clear that a ratio involving these species is the only reasonable discriminator in practice. The mean and median ratios reported here should apply for any telescope as long as the effect of beam filling can be ignored. However, HCN/SiO line intensity ratios should be established for higher–frequency lines.

5) The HCN($J = 1 \rightarrow 0$)/SiO($J = 2 \rightarrow 1$) intensity ratio increases with the mass loss rate for O–CSEs. This explains the large range in this intensity ratio without invoking for instance a spread in C/O–ratios for the M–stars. In principle, this distance–independent quantity could be used as a mass loss rate measure for O–CSEs, but the large spread in the ratio and the weak dependence on the mass loss rate make it less useful.

6) The HCN($J = 1 \rightarrow 0$) and SiO($J = 2 \rightarrow 1$) intensity ratios with respect to CO($J = 1 \rightarrow 0$) are not perfect discriminators. Despite the few detections of CS($J = 2 \rightarrow 1$) and SiS($J = 5 \rightarrow 4$) in O–CSEs we conclude that the same applies for these lines, as well as for the SiS($J = 5 \rightarrow 4$)/SiO($J = 2 \rightarrow 1$) intensity ratio.

7) The SO($J_K = 3_2 \rightarrow 2_1$) and CO($J = 1 \rightarrow 0$) intensities are tightly correlated, suggesting that SO lines may be used as good mass loss rate estimators.
8) The HCN($J = 1 \rightarrow 0$) line exhibits maser features in low-$\dot{M}$ C–CSEs. We suggest that the strongest maser features are due to radial amplification in the $F = 2 \rightarrow 1$ transition, with possibly additional radial amplification in the $F = 1 \rightarrow 1$ transition.

Acknowledgements. We are grateful to Franz Kerschbaum for supplying us with distances to the M–stars. The Swedish-ESO Submillimetre Telescope, SEST, is operated jointly by ESO and the Swedish National Facility for Radio Astronomy, Onsala Space Observatory at Chalmers University of Technology. Financial support from the Swedish Natural Science Research Council (NFR) is acknowledged.

References

Bachiller R. Fuente A., Bujarrabal V., et al. 1997 A&A 319, 235
Bedijn P.J. 1987, A&A 186, 136
Benson P.J., Little–Marenin I.R., Woods T.C., et al. 1990, ApJS 74, 911
Bieging J.H., Latter W.B. 1994, ApJ 422, 765
Bujarrabal V., Cernicharo J. 1994, A&A 288, 551
Bujarrabal V., Fuente A., Omont A. 1994a, A&A 285, 247
Bujarrabal V., Fuente A., Omont A. 1994b, ApJ 421, L47
Carlstrom J.E., Welch W.J., Goldsmith P.F., Lis D.C. 1990, AJ 100, 213
Charnley S.B., Latter W.B. 1997, MNRAS 287, 538
Charnley S.B., Tielens A.G.G.M., Kress M.E. 1995, MNRAS 274, L53
Cherchneff I., Barker J.R. 1992, ApJ 394, 703
Cherchneff I., Glassgold A.E. 1993, ApJ 419, L41
Engels D., Heske A. 1989, A&AS 81, 323
Glassgold A.E., Huggins P.J. 1983, MNRAS 203, 517
Glassgold A.E., Omont A., Guélin M. 1992, ApJ 396, 115
Groenewegen M.A.T. 1994, A&A 290, 531
Groenewegen M.A.T., Baas F., de Jong T., Loup C. 1996, A&A 306, 241
Guilloteau S., Omont A., Lucas R. 1987, A&A 176, L24
Huggins P.J., Glassgold A.E. 1982, ApJ 252, 201
Izumiura H. 1990, PhD Thesis, Tokyo University
Izumiura H., Ukita N., Kawabe R., et al. 1987, ApJ 323, L81
Izumiura H., Ukita N., Tsuji T. 1995, ApJ 440, 728
Justtanont K., Skinner C.J., Tielens A.G.G.M. 1994, ApJ 435, 852
Kahane C., Jura M. 1994, A&A 290, 183
Kastner J.H. 1992, ApJ 401, 337
Kerschbaum F., Hron J. 1996, A&A 308, 489
Kerschbaum F., Olofsson H., Hron J. 1996, A&A 311, 273
Kholopov P.N., et al. 1985, General Catalogue of Variable Stars, 4:th ed., Moscow Publishing House, Moscow
Kwan J., Webster Z. 1993, ApJ 419, 674
Lafont S., Lucas R., Omont A. 1982, A&A 106, 201
Lambert D.L., Gustafsson B., Eriksson K., Hinkle K.H. 1986, ApJS 62, 373
Larsen F., Olofsson H., Eriksson K., Gustafsson B. 1997, in prep.
Lindqvist M., Lucas R., Olofsson H., Omont A., Eriksson K., Gustafsson B. 1996, A&A 305, L57
Lindqvist M., Nyman L-Å., Olofsson H., Winnberg A. 1988, A&A 205, L15
Lindqvist M., Olofsson H., Winnberg A., Nyman L-Å. 1992, A&A 263, 183
Loup C., Forveille T., Omont A. Paul J.F. 1993, A&AS 99, 291
Lucas R., Bujarrabal V., Guilloteau S., et al. 1992, A&A 262, 491
Lucas R., Cernicharo J. 1989, A&A 218, L20
Lucas R., Guilloteau S. 1992, A&A 259, L23
Lucas R., Guilloteau S., Omont A. 1988, A&A 194, 230
Millar T.J., Herbst E. 1994, A&A 288, 561
Millar T.J., Olofsson H. 1993, MNRAS 262, L55
Nejad L.A.M., Millar T.J. 1987, A&A 183, 279
Nejad L.A.M., Millar T.J. 1988, MNRAS 230, 79
Nercessian E., Guilloteau S., Omont A., Benayoun J.J. 1989, A&A 210, 225
Netzer N., Knapp G.R. 1987, ApJ 323, 734
Nyman L.-Å., Booth R.S., Carlström U., et al. 1992, A&AS 93, 121
Nyman L.-Å., Olofsson H. 1985, A&A 150, 169
Nyman L.-Å., Olofsson H. 1997, in prep.
Nyman L.-Å., Olofsson H., Johansson L.E.B., Booth R.S., Carlström U., Wolstencroft R., et al. 1993, A&A 269, 377
Olnon F.M., Raymond E., eds of IRAS LRS Atlas, 1986, A&ASS 65, 607
Olofsson H. 1997a, The Neutral Envelopes around AGB and Post–AGB Objects: Circumstellar Molecules. In: van Dishoeck E.F. (ed.) Proc. IAU Symp. 178, Molecular Astrophysics: Probes & Processes. Kluwer, Dordrecht, p. 457
Olofsson H. 1997b, ApSS, 245, 169
Olofsson H. 1997c, The Neutral Envelopes around AGB and Post–AGB Objects: Their Structure and Evolution. In: Wing R. (ed.) Proc. IAU Symp. 177, The Carbon Star Phenomenon. Kluwer, Dordrecht, in press
Olofsson H., Bergman P., Eriksson K., Gustafsson B. 1996, A&A 322, 587
Olofsson H., Eriksson K., Gustafsson B., Carlström U. 1993a, ApJS 87, 267
Olofsson H., Eriksson K., Gustafsson B., Carlström U. 1993b, ApJS 87, 305
Olofsson H., Lindqvist M., Nyman L–Å., Winnberg A., Nguyen–Q–Rieu 1991, A&A 245, 611
Omont A., Lucas R., Morris M., Guilloteau S. 1993, A&A 267, 490
Sahai R. 1990, ApJ 362, 652
Sahai R., Bieging J.H. 1993, AJ 105, 595
Sahai R., Wannier P.G. 1992, ApJ 394, 320
Scalo J.M, Slavsky D.B. 1980, ApJ 293, L73
Sopka R.J., Olofsson H., Johansson L.E.B., Nguyen–Q–Rieu, Zuckerman B. 1989, A&A 210, 78
Truong–Bach, Nguyen–Q–Rieu 1989, A&A 214, 267
Tsuji T. 1964, Ann. Tokyo Astron. Obs., 2nd ser. 9, 1
Tsuji T. 1973, A&A 23, 411
van der Veen W.E.C.J., Habing H.J, 1988, A&A 194, 125
van der Veen W.E.C.J., Rugers M. 1989, A&A 226, 183
van Dishoeck E.F. 1988, Photodissociation and Photoionization Processes. In T.J. Millar and D.A. Williams (eds) Rate Coefficients in Astrochemistry. Kluwer, Dordrecht, p. 49
Whitelock P., Menzies J., Feast M., et al. 1994, MNRAS 267, 711
Willacy K., Millar T.J. 1997, A&A 324, 237

This article was processed by the author using Springer-Verlag LaTeX A&A style file *L-AA* version 3.